Results from a Ca-Al alloy intermetallic phase distribution

Raymond Browning 2/5/2015

These results are taken from the publication:

R. Browning, Vector potential photoelectron microscopy: hyperspectral image processing and super-resolution applied to images of a Ca–Al alloy intermetallic phase distribution, Surface and Interface Analysis, 47; pages 63–76, (2015) DOI: 10.1002/sia.5667

The images sets presented here were created using 1.0 eV electrons in a 2 T field, implying an edge resolution of 1.5 µ. However, this estimate for the edge resolution underestimates the amount of spatial information in a VPPEM image, and in fact better than 0.3 microns was achieved after deconvolution.

The sample used for these experiments is a cross section through a 3.0 mm 9%-Ca/Al metal matrix wire. The metal matrix has possible applications in overhead power transmission lines. Addition of calcium to aluminum alloy systems has both beneficial and deleterious effects. The alloy is lightweight, and has a low electrical resistance. The metal matrix is strengthened by a high distortion process which forms long filaments of Ca in the aluminum. Overheating causes intermetallics to form which reduces the strength. The sample used here has been annealed at 350^{o} C for 4 hours forming intermetallic phases, and possible spheroidization of the Ca filaments .

After registration of the image stack, multiple spectra from different regions of the images were compared and the extrema spectra found as shown in Fig. 1. These two spectra show the most extreme variation, and are defined as the endpoints: E1 for high calcium, and E2 for high aluminum (oxygen).

Two endpoint images based on E1 and E2 were created using the RMS method discussed in the paper. These images were then deconvolved using the in-house Lucy-Richardson algorithm with 50 iterations. Fig. 2 shows an area from the E1 and E2 images. Fig. 2 a, b are the E1 and E2 images and Fig. 15 c, d are the deconvolved images.

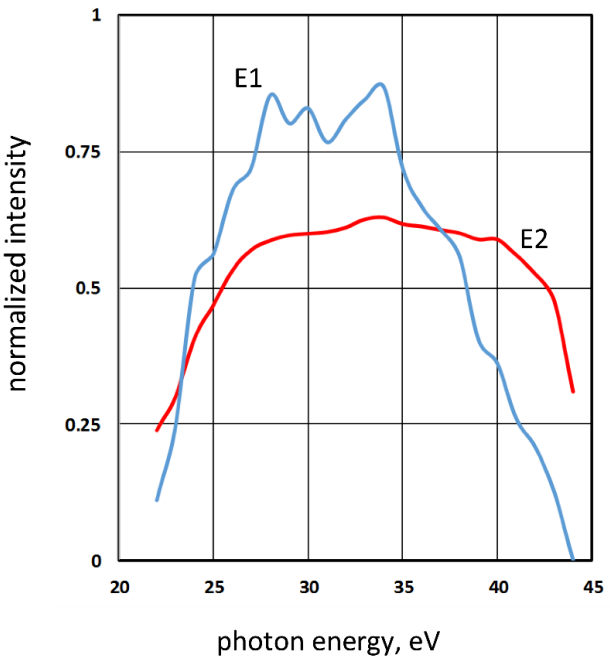

Fig. 1 Spectra identified as endpoints E1 and E2

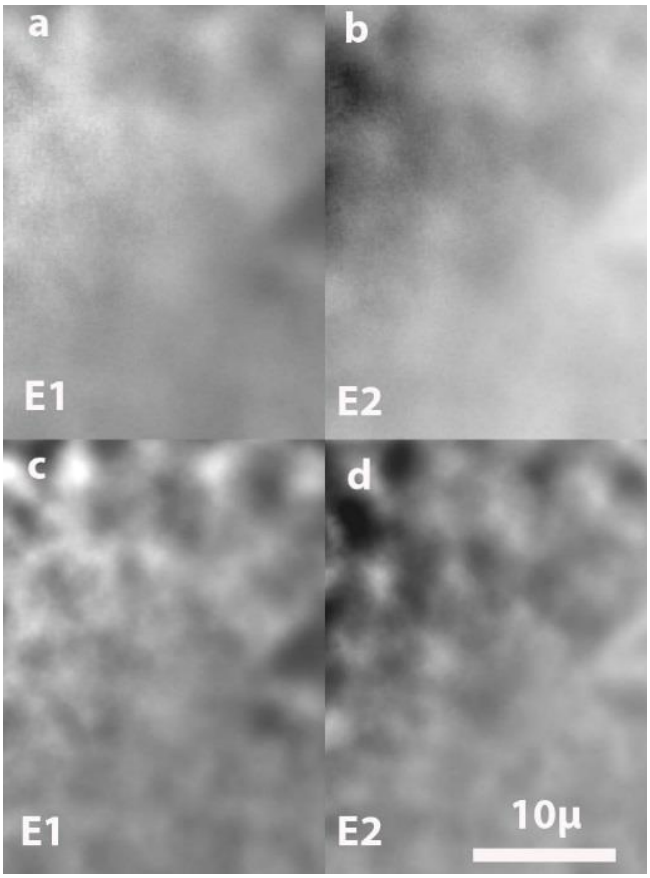

Fig. 2 Endpoint images a) E1, b) E2, c) and d) E1 and E2 deconvolved using 50 iterations of the Lucy-Richardson method

This area has a mix of features, and the endpoint images E1 and E2 are strongly anticorrelated with a similar overall variance. Because, the main direction of the two dimensional scatter diagram of E1-E2 is along a 45° line, by rotating the scatter diagram, we can effectively create a one dimensional histogram along the main axis of the variance, and still capture most of the significant information. Fig. 3 shows the scatter diagram, and histogram from the central part of the images of Fig. 2 c,d.

There are several peaks in the histogram of Fig. 3 which are indications of discrete clusters in the scatter diagram. Moreover, the scatter diagram is a narrow irregular shape which implies there is sufficient signal-to-noise across the histogram to resolve these peaks.

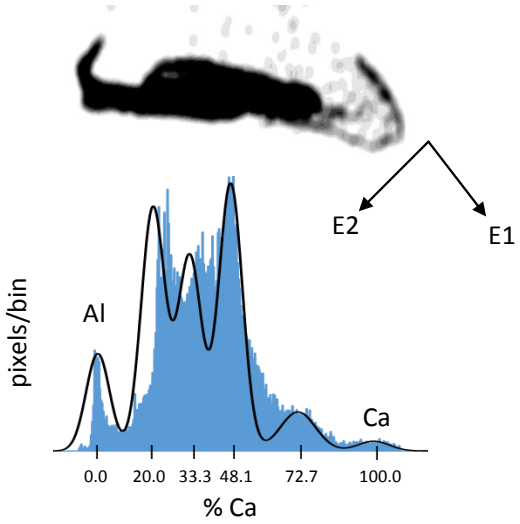

Fig. 3 Scatter diagram, and histogram from the deconvolved E1 and E2 images 2 c,d

We will make the Al-Ca phase diagram the basis for our analysis. We will assume that the bright areas in image E1 from Fig. 2 are representative of Ca, and the bright areas in E2 represent Al. We can window these bright areas in the images of Fig. 2c,d. The centers of the peaks in the windowed area histograms are then assigned to Al and Ca. The percentages of Ca in the four different intermetallic phases in the Al-Ca binary system is given in Table 1. We will assume that the signal across the histogram is a linear mixture of the E1 and E2 signals, and this represents a linear mixture of Ca and Al respectively. An illustrative fit to the histogram using these percentages is shown as the solid line in Fig. 3.

Phase	% Ca
Al	0
Al_4Ca	20
Al_2Ca	33.3
$Al_{14}Ca_{13}$	48.1
Al_3Ca_8	72.7
Ca	100

Table 1 Phase compositions in the binary Al-Ca system

The fit of Fig. 3 to the percentages of table 1 is moderate, the peak positions of Al_4Ca and Al_2Ca need some adjustment. A false color image that is based on an adjusted fit is shown in Fig. 4a. The adjusted fits give Al_4Ca at 24% and Al_2Ca at 36%. For the Fig. 4a image the divisions between the colors are made equidistant between the adjusted peaks. Al is colored red, Ca is colored blue. It is also useful to look at the overlap between the peaks, and Fig. 4b shows the 20-80% boundaries between the peaks.

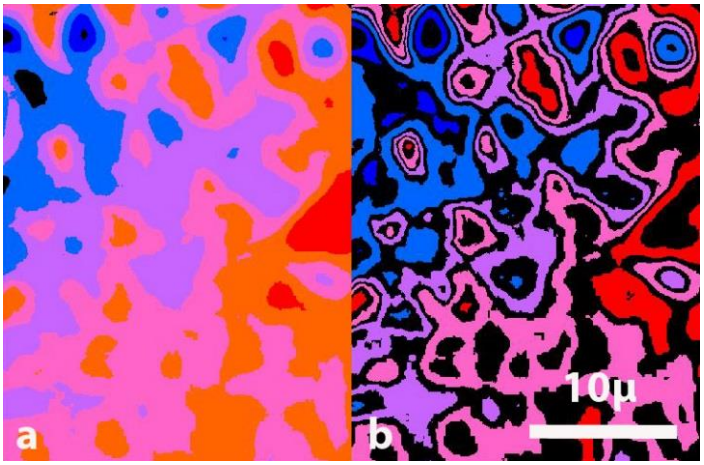

Fig. 4 False color images based on the adjusted fit to the Al-Ca phase diagram a) peak areas b) 20-80% boundary areas

In Fig. 4 the Ca and Al are seen to have formed an extended reaction zone and the long extruded Ca filaments appear to be rounded in cross section, possibly having formed spheroids. All four peaks assigned to the intermetallics are represented in the image, as well as the Al and Ca. This is a particularly dense, and detailed areas of the sample.

However, Fig. 4 is not a complete breakdown of the signal. From Fig. 4b, it can be seen that size of the boundaries are uneven. In several parts of the image, the boundaries become fairly broad. This suggests that an adjustment of

the peak positions, or further division of the histogram is required. In fact, for Fig. 3 an area in the center of the image was specifically chosen to exclude these broader regions. In Fig. 5 are the scatter diagram, and histograms from several areas where the boundaries are found to be larger in the image Fig 4b.

In the histogram in the lower half of Fig. 5 the several areas with broader boundaries have been windowed out separately, and superimposed on the histogram from Fig. 3. The histograms for these added regions have been scaled up to make them more visible. We see there are extra peaks in these broader regions. These extra peaks are colored, light blue, dark blue, and yellow in the histogram. The same regions are similarly colored in the scatter diagram at the top of Fig. 5.

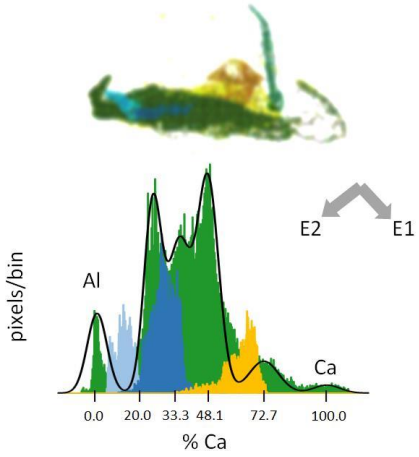

Fig. 5 Scatter diagram, and histograms from several areas in the endpoint images of Fig. 2 c,d

A void is also present. Voids are a feature of the deformation forming process. The signature of the void is the long tail pointing upwards in the scatter diagram, towards both low E1 and low E2. The void is seen as the black region in the upper left of Fig. 4a. In the histogram of Fig. 3, this peak has been suppressed. From the scatter diagram of Fig. 5, it can be seen that the yellow peak can be separated out. This peak is off the main axis of the scatter diagram towards both lower Al and Ca. Although the other two additional peaks are not well separated Fig. 6 shows an image where the regions of the additional peaks in the scatter diagram have been windowed out and imaged.

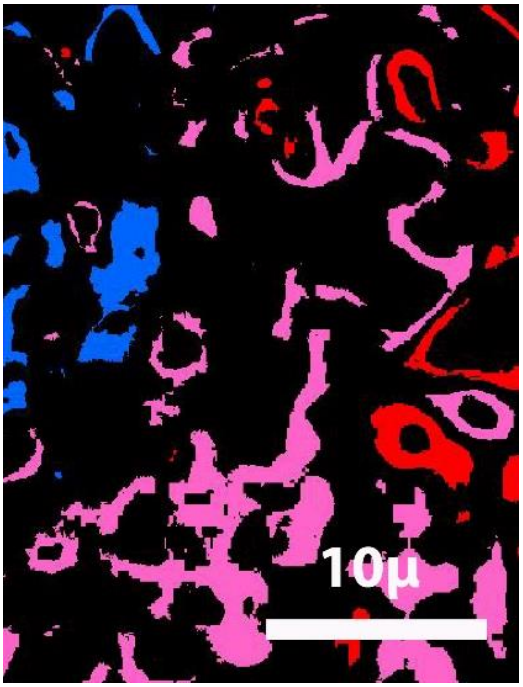

Fig. 6 Additional peak areas: red closer to Al, blue closer to Ca

The false colors of Fig. 6 follow the scheme from red towards the Al end of the distribution to blue towards the Ca end. Therefore, the yellow peak in Fig. 5 is imaged in blue as it closer to Ca. As can be seen, the additional peak areas are clumpy, and not boundary like. Unfortunately, there is insufficient data to determine what these extra features are. The peaks could be surface phases, or might represent bulk phases that includes contaminants from the alloy manufacturing process.

The presence of the void gives an opportunity to measure the edge response, and estimate the spatial resolution. By windowing across the scatter diagram of Fig. 5 to capture just the additional yellow peak, and that part of the void signature that is horizontal to it, we find they share a common boundary. Measuring the 20-80% response gives a conservative spatial resolution of 0.3 µ.

A spatial resolution of 0.3 µ confirms that the composition of the larger areas in Figs. 4 and 6 are not simply unresolved spatial overlap from a mixture of the end components. The peaks that are seen in the histograms are real compositional clusters. Therefore, the four main intermediate regions could reasonably correspond to the four intermetallic regions in the Al-Ca phase diagram. Fig. 7 is an annotated image of the phase distribution using this

reasoning as a basis. The larger areas the additional peaks in Fig. 6 have been removed.

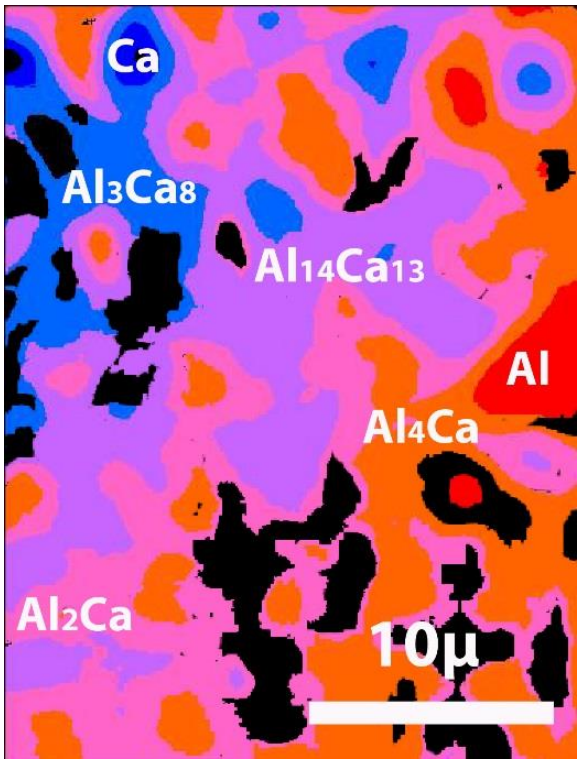

Fig. 7 VPPEM phase image of Al-Ca alloy

The presence of the Al-Ca intermetallics seems well established, and these intermetallics might be the source of the large variations in workfunction on the freshly cleaned samples. There is a possible 2.0 eV difference in work function between Al_4Ca and Al. The results are consistent with previous analysis using backscattered electron microscopy, energy dispersive spectroscopy (EDS), and x-ray diffraction (XRD). Although these present results differ in that more phases have been isolated in the images. However, with the low spectral resolution, we cannot spectroscopically identify the chemistry of the intermetallics or any of the additional features. Further, we can only loosely associate Al 2p spectra with these images as we have failed to register the image stack across the two spectral regions. We have also made several assumptions to reach this point. These we have not been able to test fully with the current data sets. While the highly detailed nature of the result is remarkable given the low photon flux, and the difficultly of image alignment, yet we cannot say this is an unambiguous analysis. Too much information is missing, both in chemical shifts, and in spectral range.

However, despite these caveats, we have the conclusion that the VPPEM technique has spatially resolved the reaction products between the Ca and Al in this metal matrix sample. The image processing steps have been successful in analyzing a relatively unknown and complex sample.

The current prototype microscope uses a 2 T magnet. There is a limited range of photon energies, and low counting statistics from beamline U4A. Achieving better than 300 nm resolution, and a detailed breakout of the phase distribution is very encouraging. In the future the magnetic field can be taken to 20 T. The microscope will be moved to the NIST soft and tender beam lines at NSLS II. These beam lines will have six orders of magnitude higher flux density, and a 100 eV to7.5 keV photon range. Many of the limitations with the present analysis will be removed, and spatial resolutions down to a few tens of nanometers are expected.